Applied Mathematical Modelling 36 (2012) 4341–4355

Contents lists available at SciVerse ScienceDirect

Applied Mathematical Modelling

journal homepage: www.elsevier.com/locate/apm

New mathematical modelling and simulation of an industrial accumulator for elastic webs

David Kuhm [a,b,c], Dominique Knittel [a,b,*]

[a] Web Handling Research Center, UFR Physique et Ingénierie, Campus Meinau, University of Strasbourg, 17, rue du Maréchal Lefebvre, 67100 Strasbourg, France
[b] Laboratoire de Génie de la Conception, INSA Strasbourg, 24 boulevard de la Victoire, 67084 Strasbourg, France
[c] Laboratoire de Physique et Mécanique Textiles ENSISA, 11, rue Alfred Werner, 68093 Mulhouse, France

ARTICLE INFO

Article history:
Received 23 May 2011
Received in revised form 9 November 2011
Accepted 15 November 2011
Available online 25 November 2011

Keywords:
Industrial accumulator
Roll-to-roll
Mathematical modelling
Performances analysis
Simulation

ABSTRACT

This paper concerns the modelling of an accumulator used in industrial elastic web processing plant such as paper mills, fabric, rolling mills etc. Accumulators are used to allow rewind or unwind core changes while the process continues at a constant web velocity. A new nonlinear model of a pneumatic actuated industrial accumulator including pneumatic jack model, static friction representation and web weight is first detailed which enables to deduce a linear model. These models are derived from physical laws that describe web tension and velocity dynamics in each web span. In a second part, the effects of time-varying mechanical parameters, such as web Young modulus, web length and rollers inertia on accumulator dynamics are presented. The performances of the modeled accumulator are illustrated by simulations in Matlab/Simulink software environment.

1. Introduction

Having continuous process lines increases the productivity of the plant. Accumulators (Fig. 1) are used to allow rewind or unwind core changes while the process continues at a constant velocity. Accumulators are composed by a lot of idle rollers and by a carriage that has to be moved in order to store or release web during the production phases. Most of the time, the accumulator carriage is maintained at its nominal position. Nevertheless, when the unwinder wound roll is almost empty, the carriage is moved up in order to increase the web length stored in the accumulator. During the unwinder roll change phase, the unwinder is stopped and the accumulator carriage is adequately moved down to release the stored web and to maintain constant web line velocity at the accumulator output. After the unwinder roll change, the carriage is moved back to its nominal position. The unwinder roll changing time has to be as short as possible being limited by the accumulated web length. Web tensions inside an accumulator are easy to master during the regular production phase (when the carriage is at its nominal position). However web tensions variations often occur in the transient phases and can generate web folds or breaks due to the inertia and friction of the idle rollers.

Different works in web tension control of roll-to-roll systems have been published in the past years. For example Zalhan and Jones [1], Brandenburg [2,3], Benlatreche et al. [4], Knittel et al. [5,6], Gassmann et al. [7], Giannoccaro et al. [8], Chen et al. [9] present the modelling and control of a continuous processing line composed only with tractors and idle rollers, whereas Wolfermann [10], Olsen [11], Gassmann [12], Knittel et al. [13] describe the unwinding and the winding process. Only few works presents the modelling and the control of industrial accumulators. Important results can be found in

* Corresponding author at: Web Handling Research Center, UFR Physique et Ingénierie, Campus Meinau, University of Strasbourg, 17, rue du Maréchal Lefebvre, 67100 Strasbourg, France. Tel.: +33 3 68 85 49 50; fax: +33 3 68 85 49 72.
E-mail address: knittel@unistra.fr (D. Knittel).

0307-904X/$ - see front matter © 2011 Elsevier Inc. All rights reserved.
doi:10.1016/j.apm.2011.11.060

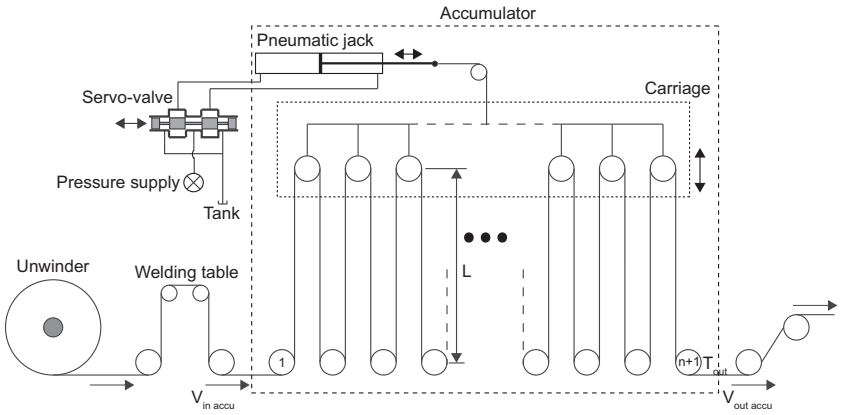

Fig. 1. Example of an industrial accumulator.

Koç et al. [14,15] who present the modelling and control of an industrial accumulator, using an empirical tension calculation law. Pagilla et al. present the dynamics and control of a hydraulic actuated accumulator in [16], but in [17] they insist that future work should include the dynamics of the actuator, coupled with the dynamics of the carriage and the web spans. In their work, they also neglected the effect of the weight. Kuhm et al. present the modelling and robust control of an industrial accumulator, neglecting the carriage actuator dynamics [18], and [19] compare the accumulator presented in this paper with a motor actuated. Knittel and Kuhm [20] concerns the accumulators controllers optimization using genetic algorithm. This paper presents for the first time a complete mathematical model of an industrial accumulator including the dynamics of the actuator and carriage.

In the next part of this paper, the detailed physically based model of the accumulator including web span weight and air cylinder representation is described. Finally, the third part of this contribution highlights the effect of mechanical parameters variations on the accumulator dynamic performances. This part also presents simulation results obtained in the Matlab/Simulink software environment for the modeled accumulator.

2. Accumulator modelling

2.1. Nonlinear model of the accumulator web dynamics

Equations describing web tension behavior between two consecutive rollers and the velocity of each roll enable to build the nonlinear model of a web transport line. Thus, the accumulator model can be constructed by assembling adequately web spans, rollers and carriage submodels.

2.1.1. Web tension calculation

Assuming no sliding between web and rollers, the equation of continuity applied to a web span between two consecutive rollers (Fig. 2), is given by relation (1) (Koç [21], Koç et al. [22]).

$$\frac{d}{dt}\left(\frac{L_k}{1+\varepsilon_k^t}\right) = -\frac{V_{k+1}}{1+\varepsilon_k^t} + \frac{V_k}{1+\varepsilon_{k-1}^t}, \tag{1}$$

where L_k is the web length between the kth and the $(k+1)$th rollers. This web length varies during the accumulator carriage motion. V_k and V_{k+1} are respectively the velocity of the kth and the $(k+1)$th rollers and ε_k^t the strain of the kth web span. Web tension T_k^t is then deduced from general web tension relation (1) by applying the Hooke's law.

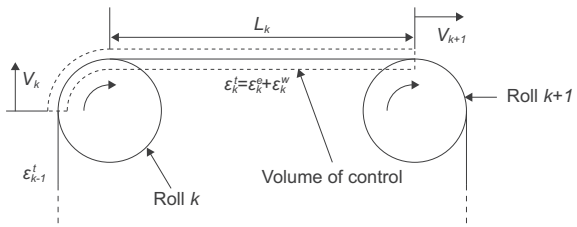

Fig. 2. Indices of web span between two consecutive rollers.

The equivalent strain ε_k^t in the web (see relation (2)) is composed by the strain ε_k^w induced by the web weight (relation (4)) and by the strain ε_k^e induced by the web elongation without the web weight:

$$\varepsilon_k^t = \varepsilon_k^e + \varepsilon_k^w. \tag{2}$$

The weight W_{L_k} of a web span is given by the following relation (Kim [23]):

$$W_{L_k} = \rho g S L_k = E S \varepsilon_k^w, \tag{3}$$

with ρ the web mass density, g the gravity, L_k the span length and E is the web Young modulus.

The strain ε_k^w in the web span resulting from the gravity is than obtained from (3):

$$\varepsilon_k^w = \frac{\rho g L_k}{E}. \tag{4}$$

In our accumulator (web with a Young modulus of 3000 MPa, a mass density of 750 kg $\cdot$ m^{-3}, a section of $9.35 * 10^{-5}$ m^2 and a nominal tension of 300 N, corresponding to a paper web) $\varepsilon_k^e \gg \varepsilon_k^w$ $(\varepsilon_k^e \cong 290\varepsilon_k^w)$.

2.1.2. Web velocity calculation

The velocity dynamics of the kth roll is calculated using the torque balance. Assuming there is no sliding between the web and the roll, the web velocity V_k is equal to the linear velocity of the roll. This velocity dynamic is given by Eq. (5):

$$\frac{d}{dt}(J_k \Omega_k) = C_{mk} - C_{rk} - C_{fk}, \tag{5}$$

where $\Omega_k = \frac{V_k}{R_k}$ is the angular velocity of the kth roll, J_k the roll inertia and R_k the roll radius. C_{mk} is the motor torque for a driven roller. $C_{rk} = R_k(T_k - T_{k-1})$ stands for the torque introduced by the web and C_{fk} is friction torque between the roll and its shaft (composed by static and dynamic friction).

The Eqs. (1) and (5) are applied to each web span and roll of the studied accumulator and enable the construction of a non-linear longitudinal web dynamics simulator.

2.2. Nonlinear model of the accumulator carriage motion

This part presents the nonlinear model of a pneumatic accumulator carriage actuator, including static frictions modelling.

2.2.1. Displacement of the accumulator carriage

In the phase of wound roll change, the accumulator output speed $V_{out\ accu}$ is maintained at nominal speed V_{ref} and the input speed $V_{\text{in accu}}$ decreases to 0. In order to maintain the output web tension and velocity constant during this change, it is necessary to move adequately the accumulator carriage. In our study, the accumulator composed of $n + 1$ rollers has n web spans. The accumulator carriage displacement speed reference during the wound roll change deduced from the following relation:

$$V_{\text{accu}} = \frac{1}{n}(V_{\text{in accu}} - V_{\text{out accu}}). \tag{6}$$

This speed reference enables to find the reference carriage position by integration.

2.2.2. Unwinding speed during the accumulation phase

During the web accumulation phase, the unwinder speed has to be increased to keep a constant web tension inside the accumulator. This unwinding speed reference is deduced from the Eq. (6):

$$V_{\text{in accu}} = nV_{\text{accu}} + V_{\text{out accu}}. \tag{7}$$

2.2.3. Pneumatic jack modelling

In the studied accumulator, carriage motion is ensured by a pneumatic jack (Figs. 1 and 3). Some works have been done in hydraulic or pneumatic systems modelling and can be found for example in Hamiti et al. [24], Zhihong and Bone [25]. Models of hydraulic systems including valves and cylinder can be found in Jelali and Kroll [26]. These models using bi-directional valves can not be implemented directly but have to be adapted to our pneumatic jack: in our air cylinder, only the chamber A of the cylinder is connected to the valve, the chamber B is directly connected to a high flow outlet, so the pressure in chamber B is supposed equal to the tank pressure.

2.2.3.1. Pressure/flow equation for a spool valve. A valve presents a lot of non linearities such as dead band, saturation, hysteresis, friction forces. The air flow across the valve can be represented essentially by relations (8) and (9) (Jelali and Kroll [26]).

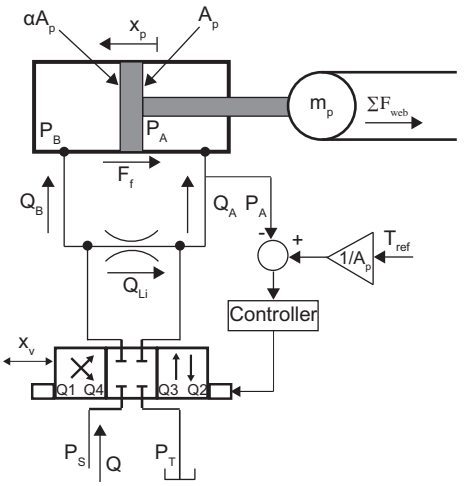

Fig. 3. Generic valve and cylinder representation including pressure regulation.

$$Q_A = Q_1 - Q_2 = C_{v1} \cdot sg(x_v) \cdot sign(P_S - P_A) \cdot \sqrt{|P_S - P_A|} - C_{v2} \cdot sg(-x_v) \cdot sign(P_A - P_T) \cdot \sqrt{|P_A - P_T|}, \tag{8}$$

$$Q_B = Q_3 - Q_4 = C_{v3} \cdot sg(-x_v) \cdot sign(P_S - P_B) \cdot \sqrt{|P_S - P_B|} - C_{v4} \cdot sg(x_v) \cdot sign(P_B - P_T) \cdot \sqrt{|P_B - P_T|}, \tag{9}$$

with

$$sg(x_v) = \begin{cases} x_v & \text{for } x_v \geqslant 0, \\ 0 & \text{for } x_v < 0, \end{cases} \tag{10}$$

$$sg(-x_v) = \begin{cases} -x_v & \text{for } -x_v \geqslant 0, \\ 0 & \text{for } -x_v < 0, \end{cases} \tag{11}$$

where x_v is the valve position determining the air flow direction. C_{vi} are the valve orifice coefficient. The different air pressure P_i and air voluminous flow Q_i are indicated on Fig. 3.

2.2.3.2. Dynamic representation of the servo-valve. The dynamic of the servo valve is calculated by the following equation (Jelali and Kroll [26]):

$$\frac{1}{\omega_v^2}\ddot{x_v} + \frac{2D_v}{\omega_v}\dot{x_v} + x_v + f_{hs} \cdot sign(\dot{x_v}) = K_v \cdot u_v, \tag{12}$$

with $\dot{x_v}$ the valve velocity and $\ddot{x_v}$ the valve acceleration. K_v is the valve gain, ω_v the valve natural frequency, D_v the valve damping coefficient and f_{hs} the valve hysteresis. These coefficients are often given by the valve manufacturer.

2.2.3.3. Pressure dynamics in cylinder chamber. The air cylinder also presents non linearities such as pressure dependent bulk modulus, saturation, friction forces. The air flow inside each cylinder chamber are represented according relation (13) and (14):

$$Q_A - Q_{Li} = \dot{V}_A + \frac{V_A}{E'(P_A)}\dot{P}_A, \tag{13}$$

$$Q_B + Q_{Li} = \dot{V}_B + \frac{V_B}{E'(P_B)}\dot{P}_B, \tag{14}$$

with V_A and V_B the volume of each chamber, including the valve connecting line. This volume are given by relations (15) and (16). Q_{Li} represents the internal flow leakage between the two chamber. V_{P1A} and V_{P1B} are the pipeline volume, S is the piston stroke, A_P is the piston section, α is the ratio between chamber A and chamber B piston surface and x_p is the piston position. $E'(P_A)$ and $E'(P_B)$ are the effective bulk modulus depending on the pressure.

$$V_A = V_{P1A} + \left(\frac{S}{2} + x_p\right)A_P, \tag{15}$$

$$V_B = V_{P1B} + \left(\frac{S}{2} - x_p\right)\alpha A_P, \tag{16}$$

$$\dot{V}_A = A_P\dot{x}_p, \tag{17}$$

$$\dot{V}_B = -\alpha A_P\dot{x}_p. \tag{18}$$

Finally from relations (13)–(18) the pressure dynamics inside each cylinder chamber is then given by:

$$\dot{P}_A = \frac{E'(P_A)}{V_A}(Q_A - A_P\dot{x}_p - Q_{Li}), \tag{19}$$

$$\dot{P}_B = \frac{E'(P_B)}{V_B}(Q_B + \alpha A_P\dot{x}_p + Q_{Li}). \tag{20}$$

2.2.3.4. Piston motion and friction representation. In order to provide the piston motion dynamics, a special attention has to be paid to static friction force F_s.

This work presents a novel approach to include static friction force F_s properly in the simulator. Static friction sign depends obviously on the direction of the piston displacement. But the key point that has to be handled is when piston velocity is zero. One has to make sure that the piston has to stand still when the force generated by pressure on the piston surface is not sufficient to exceed the static friction force. These conditions are summarized in (22).

From Fig. 3, the equation of the piston motion is then deduced from the second Newton law applied to the piston.

$$\begin{cases} m_t\ddot{x}_p = (P_A - \alpha P_B)A_P - F_{ext} - F_{fv}(\dot{x}_p) - F_{fs} - m_t g & \text{if } B_1 \text{ or } B_2 \text{ satisfied} \\ m_t\ddot{x}_p = (P_A - \alpha P_B)A_P - F_{ext} - F_{fv}(\dot{x}_p) + F_{fs} - m_t g & \text{if } B_3 \text{ or } B_4 \text{ satisfied} \\ m_t\ddot{x}_p = 0 \quad \text{else.} \end{cases} \tag{21}$$

where m_t is the total mass including carriage and piston, F_{ext} are the forces applied by the web spans on the carriage, F_{fv} and F_{fs} stand for viscous and static frictions.

A simulation of the piston motion (using arbitrary pressure and forces) is given in Fig. 17 in appendix. At the beginning, we can see that in the case the force generated by the pressure on the piston is less that static friction force F_{fs}, the piston does not move (zone A).The piston only starts to move when the forces applied on the piston are higher that the friction force (zone B). In the case the piston is moving and the applied forces are lower that the friction force, the piston will decelerate (zone C) until the piston gets to a velocity equal to zero (zone D). This is observed for both moving direction of the piston (see also zone E).

$$\begin{cases} B_1 : (P_A - \alpha P_B)A_P - F_{web} - m_t g > F_{fs} \\ B_2 : \qquad\qquad \dot{x}_p > \varepsilon\dot{x}_p \\ B_3 : (P_A - \alpha P_B)A_P - F_{web} - m_t g < -F_{fs} \\ B_4 : \qquad\qquad \dot{x}_p < -\varepsilon\dot{x}_p. \end{cases} \tag{22}$$

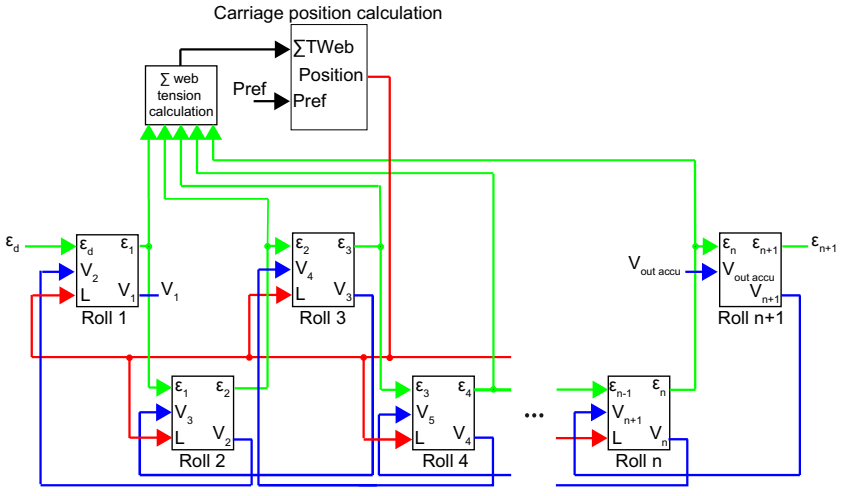

Fig. 4. Matlab/Simulink accumulator representation.

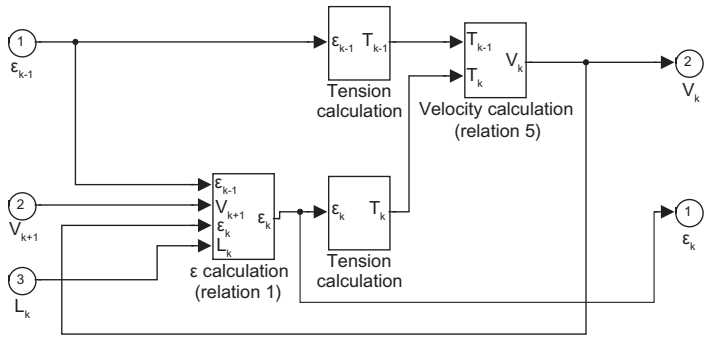

Fig. 5. Detail of an accumulator roll modelling in Matlab/Simulink.

2.2.3.5. Jack pressure regulation. In order to achieve the expected force that has to be applied on the carriage, the pneumatic jack uses a pressure regulation. The control scheme is illustrated on Fig. 3. The reference force T_{ref} is deduced from the nominal tension desired in the accumulator and has also to compensate the carriage weight, because the modelled accumulator is a vertical one.

$$T_{ref} = nT_{\text{web ref}} + m_t g. \tag{23}$$

2.2.3.6. Simulator building in the Matlab/ Simulink software environment. The blocks scheme shown in Fig. 4 highlights the multiple interaction of the different subsystems that compose the accumulator. The details of a roll dynamic modelling is given in Fig. 5.

2.3. Linear model of the accumulator

2.3.1. Linearization

The linear model is deduced from the nonlinear one around a setting point and can be described by a state space representation. The web span dynamic (see relation (1)) linearization is detailed in Koç [21] and Kuhm et al. [18]. The linear model is obtained by linearizing an accumulator including an "ideal" carriage actuator (neglecting the nonlinear terms: static friction, dead band, pressure dependant bulk modulus and saturations), according to the scheme given on Fig. 6. The linear model is useful for the frequency analysis of the transfer function (bode diagrams calculation). As seen in the precedent part of this paper, $\varepsilon_k^e \gg \varepsilon_k^w$, so in this study, the web weight can be neglected. However in other case, such as accumulators designed for metallic webs, the web weight is significative and has to be taken into account by keeping the web weight terms during the linearization.

By derivating and developing relation (1) describing the web tension, relation (24) is obtained.

$$\frac{-L_k}{(1+\varepsilon_k)^2}\frac{d\varepsilon_k}{dt} = -\frac{V_k+1}{1+\varepsilon_{k+1}} + \frac{V_k}{1+\varepsilon_{k-1}} - \frac{1}{1+\varepsilon_k}\frac{dL_k}{dt}. \tag{24}$$

Using the classical approximation (25) and by keeping only the first order terms, the relation after simplification can be written as following:

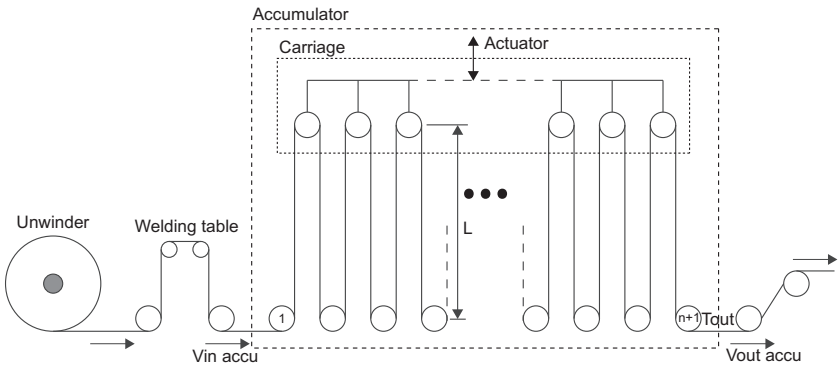

Fig. 6. Ideal accumulator scheme.

$$\frac{1}{1+\varepsilon_k} \approx 1-\varepsilon_k, \tag{25}$$

$$L_k \frac{d\varepsilon_k}{dt} = V_{k+1}(1+\varepsilon_k) - V_k(1+2\varepsilon_k-\varepsilon_{k-1}) + \frac{dL_k}{dt}(1+\varepsilon_k). \tag{26}$$

An example of the developed relation with linearization before derivation and therefore less accurate, including web weight can be found in [23]. Introducing the Hooke's law into relation (26), leads finally to the tension dynamics description:

$$L_k \frac{dT_k}{dt} = V_{k+1}(ES+T_k) - V_k(ES+2T_k-T_{k-1}) + \frac{dL_k}{dt}(ES+T_k). \tag{27}$$

The relation (27) can be linearized around the nominal web tension T_0 and nominal velocity V_0 with $T_k = T_0 + t_k$, $T_{(k-1)} = T_0 + t_{(k-1)}$, $V_k = V_0 + v_k$ and $V_{(k+1)} = V_0 + v_{(k+1)}$. By keeping only the first order terms, Eq. (27) can be written as:

$$\frac{dt_k}{dt} = \frac{E_0}{L_k} v_{k+1} - \frac{E_0}{L_k} v_k - \frac{V_0}{L_k} t_k + \frac{V_0}{L_k} t_{k-1} + \frac{E_0}{L_k} \frac{dL_k}{dt}, \tag{28}$$

where $E_0 = ES + T_0$

The web speed is deduced from relation (5):

$$\frac{dv_k}{dt} = -\frac{R_k^2}{J_k} t_{k-1} - \frac{F_k}{J_k} v_k + \frac{R_k^2}{J_k} t_k, \tag{29}$$

where F_k the friction coefficient between the kth roll and its shaft.

2.3.2. State space representation of the accumulator

The linear model of the accumulator is described by a state space representation given in (30) and (31). The states are the tension and velocity in each web span. The state space model has three inputs $\left(\frac{dL}{dt}, V_d, V_{\text{out accu}}\right)$ and one output T_{n+1}, the accumulator output tension. The input u is the carriage displacement velocity, whereas V_d is the unwinder speed and $V_{\text{out accu}}$ the velocity after the accumulator output. L is the web span length in the accumulator (related to carriage position).

$$\begin{cases} \dot{X} = \left(A + \frac{A_1}{L}\right)X + \frac{B}{L}u + B_1 v, \\ Y = CX + Du, \end{cases} \tag{30}$$

where

$$X = \begin{bmatrix} T_d \\ V_a \\ T_a \\ V_{a1} \\ T_{a1} \\ \vdots \\ V_{n+1} \\ T_{n+1} \end{bmatrix} \quad u = \frac{dL}{dt} \quad v = \begin{pmatrix} V_d \\ V_{\text{out accu}} \end{pmatrix}. \tag{31}$$

The matrices A, A_1, B, B_1, C and D are as follow:

$$A = \begin{pmatrix} \frac{-v_0}{L_d} & \frac{E_0}{L_d} & 0 & 0 & 0 & 0 & 0 & 0 & 0 & \cdots & 0 \\ \frac{-R_a^2}{J_a} & \frac{-f_a^2}{J_a} & \frac{R_a^2}{J_a} & 0 & 0 & 0 & 0 & 0 & 0 & \cdots & 0 \\ \frac{v_0}{L_a} & \frac{-E_0}{L_a} & \frac{-v_0}{L_a} & \frac{E_0}{L_a} & 0 & 0 & 0 & 0 & 0 & \cdots & 0 \\ 0 & 0 & \frac{-R_{a1}^2}{J_{a1}} & \frac{-f_{a1}^2}{J_{a1}} & \frac{R_{a1}^2}{J_{a1}} & 0 & 0 & 0 & 0 & \cdots & 0 \\ 0 & 0 & 0 & 0 & 0 & 0 & 0 & 0 & 0 & \cdots & 0 \\ 0 & 0 & 0 & 0 & \frac{-R_{a2}^2}{J_{a2}} & \frac{-f_{a2}^2}{J_{a2}} & \frac{R_{a2}^2}{J_{a2}} & 0 & 0 & \cdots & 0 \\ 0 & 0 & 0 & 0 & 0 & 0 & 0 & 0 & 0 & \cdots & 0 \\ \vdots & \vdots & \vdots & \vdots & \vdots & \ddots & \ddots & \ddots & \ddots & 0 & 0 \\ 0 & 0 & 0 & 0 & 0 & \cdots & 0 & 0 & 0 & 0 & 0 \\ 0 & 0 & 0 & 0 & 0 & \cdots & 0 & 0 & \frac{-R_{an+1}^2}{J_{an+1}} & \frac{-f_{an+1}^2}{J_{an+1}} & \frac{R_{an+1}^2}{J_{an+1}} \\ 0 & 0 & 0 & 0 & 0 & \cdots & 0 & 0 & \frac{v_0}{L_{an+1}} & \frac{-E_0}{L_{an+1}} & \frac{-v_0}{L_{an+1}} \end{pmatrix}, \tag{32}$$

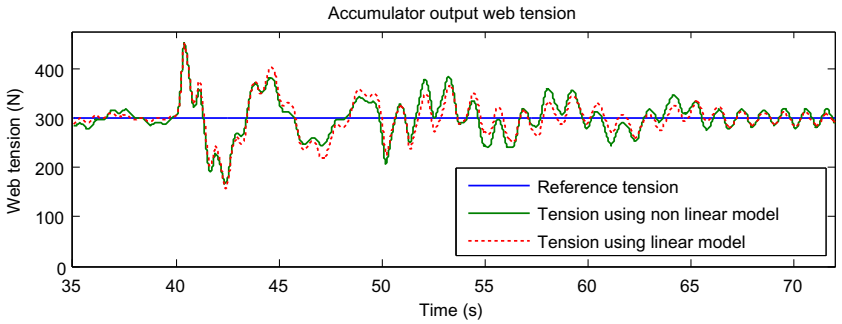

Fig. 7. Linear and non linear models comparison during web span length variations.

$$A_1 = \begin{pmatrix} 0 & 0 & 0 & 0 & 0 & 0 & 0 & 0 & 0 & \cdots & 0 \\ 0 & 0 & 0 & 0 & 0 & 0 & 0 & 0 & 0 & \cdots & 0 \\ 0 & 0 & 0 & 0 & 0 & 0 & 0 & 0 & 0 & \cdots & 0 \\ 0 & 0 & 0 & 0 & 0 & 0 & 0 & 0 & 0 & \cdots & 0 \\ 0 & 0 & v_0 & -E_0 & -v_0 & E_0 & 0 & 0 & 0 & \cdots & 0 \\ 0 & 0 & 0 & 0 & 0 & 0 & 0 & 0 & 0 & \cdots & 0 \\ 0 & 0 & 0 & 0 & v_0 & -E_0 & -v_0 & E_0 & 0 & \cdots & 0 \\ \vdots & \vdots & \vdots & \vdots & \vdots & \ddots & \ddots & \ddots & \ddots & 0 & 0 \\ 0 & 0 & 0 & 0 & 0 & \cdots & v_0 & -E_0 & -v_0 & E_0 & 0 \\ 0 & 0 & 0 & 0 & 0 & \cdots & 0 & 0 & 0 & 0 & 0 \\ 0 & 0 & 0 & 0 & 0 & \cdots & 0 & 0 & 0 & 0 & 0 \end{pmatrix}, \tag{33}$$

$$B^T = (0 \quad 0 \quad 0 \quad 0 \quad E_0 \quad 0 \quad E_0 \quad \cdots \quad E_0 \quad 0 \quad 0) \tag{34}$$

$$B_1^T = \begin{pmatrix} 0 & 0 & 0 & 0 & 0 & 0 & 0 & \cdots & 0 & 0 & \frac{E_0}{L_{an}} \\ \frac{-E_0}{L_d} & 0 & 0 & 0 & 0 & 0 & 0 & \cdots & 0 & 0 & 0 \end{pmatrix}, \tag{35}$$

$$C = (0 \quad 0 \quad 0 \quad 0 \quad 0 \quad 0 \quad 0 \quad \cdots \quad 0 \quad 0 \quad 1,) \tag{36}$$

$$D = 0. \tag{37}$$

The state matrix A_1 and the input matrix B are related to the variable web length L between two consecutive rollers (see relation (28)). Fig. 7, shows that the linear model fits on the non linear one, even if the linearization neglects some nonlinearities. Therefore, the linear model can be used on the one hand to study the frequency response of the system and on the other hand to synthesize linear controllers.

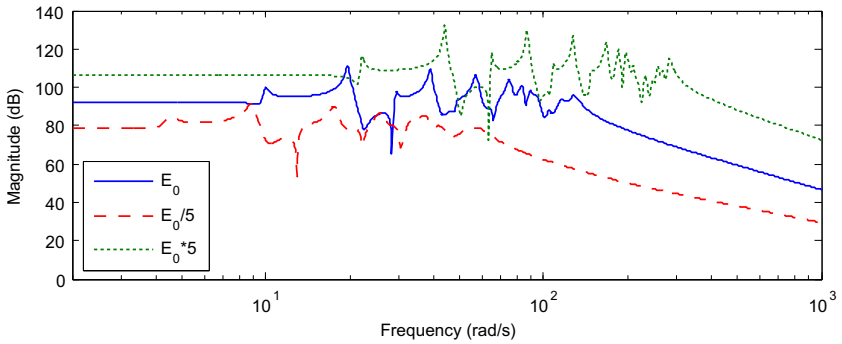

Fig. 8. Bode diagram of W_2 for different Young modulii.

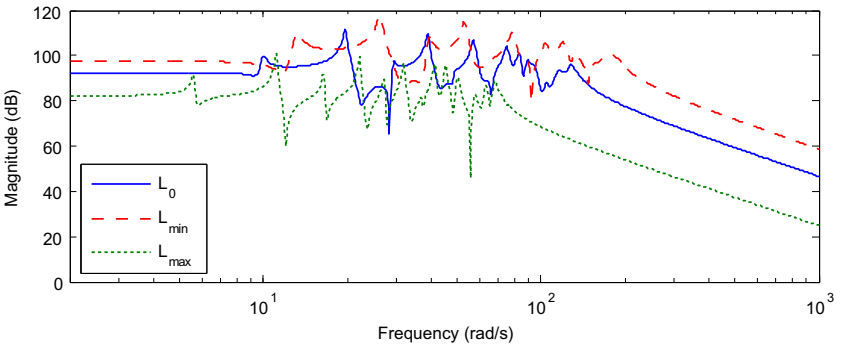

Fig. 9. Bode diagram of W_2 for different web span lengths.

3. Accumulator performances analysis

3.1. Influence of the mechanical parameters

Depending on the type of accumulator, mainly two control strategies are applied: one using $V_{in\ accu}$ as control signal (controller output), the other using L (see Fig. 1). Using this two control signals in our approach leads to the calculation of two transfer functions: the first one between the accumulator output tension T_{out} and the accumulator input velocity $V_{in\ accu}$ named W_1 and the second one between T_{out} and the web span length L named W_2.

In the following parts, the influences of the most significant physical parameter variations around their nominal values are analyzed on simulated Bode diagrams.

3.1.1. Influence of the web elasticity modulus

The web elasticity influences the web dynamics (tension and velocity) not only in the transient phases but also in steady state. One can observe on Fig. 8 that both the static gain and the resonances (gains and frequencies) are depending on the Young modulus. The same observations have been made for the transfer functions W_1 and W_2. In the industry, often Young modulus changes occur during the manufacturing process and therefore the control performances are reduced if the controllers are not enough robust for such variations. Consequently, the controllers have to be adjusted/calculated for each range of web elasticity, or robust for a given web elasticity range.

3.1.2. Variation of span lengths

Like the Young modulus, the web span length in the accumulator (related to the position of the carriage) has a significant influence on the web dynamic (Fig. 9). A long web span will have weaker resonance frequencies and a lower static gain. The same observation has been made for both transfer functions W_1 and W_2. Therefore the dynamic sensitivity to web length variations has to be taken into account during the controller synthesis (the web span length is varying each time when a wound roll change occurs).

3.1.3. Roll inertias influence

The idle rollers inertias also influence the web dynamics. As we can observe on Fig. 10, these inertias should be as weak as possible. Indeed important inertias strongly decrease the bandwidth of the system; this reduced bandwidth will make it difficult to control the accumulator. On the contrary, the inertias have no effect on the static gain. These observations have been made for both transfer functions W_1 and W_2.

3.1.4. Influence of nominal velocity

The nominal web velocity does not influence the system bandwidth (see Fig. 11). But a high web speed reduces the magnitude of the resonance peaks of the transfer functions. This effect does not depend on the web span length.

3.1.5. Influence of other parameters

The shaft/roller frictions have minor effect on the system bandwidth (see Fig. 12). A change of the friction value during the production will thus have a minor influence on the controller performances. The nominal tension does not have also any effect on the accumulator bandwidth and on the resonance peaks (see Fig. 13). This has been observed for both transfer functions W_1 and W_2.

3.1.6. Remarks

The previous part clearly shows that the most important parameters which influence our industrial accumulator dynamics are the web Young modulus, the roller inertias and the web span length.

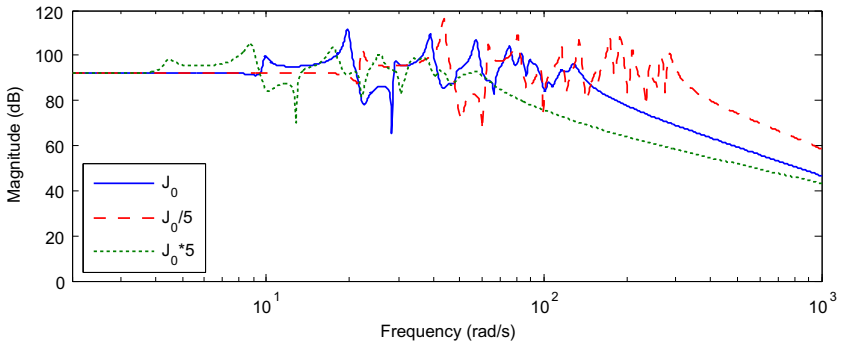

Fig. 10. Bode diagram of W_2 for different rollers inertias.

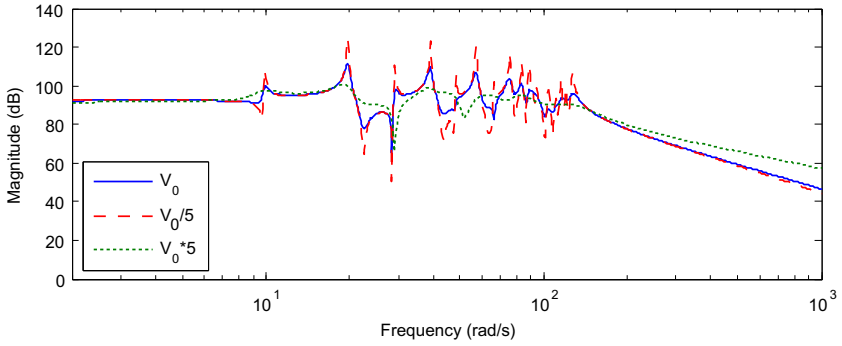

Fig. 11. Bode diagram of W_2 for different nominal velocities.

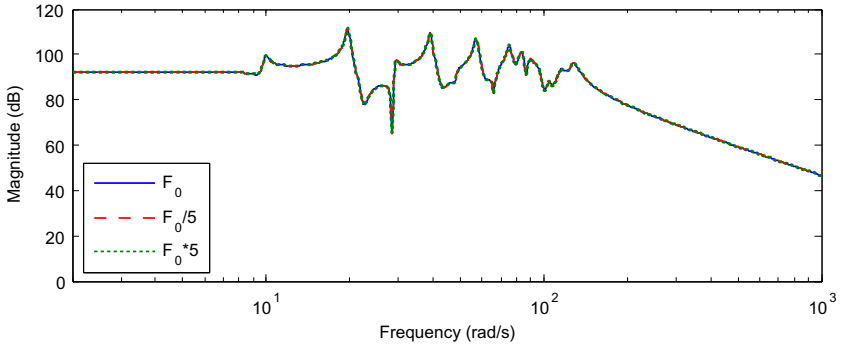

Fig. 12. Bode diagram of W_2 for different friction forces.

3.2. Control strategy

As mentioned previously, the accumulator can be controlled in two different ways: the controller can operate either on the input velocity or the web span length. More precisely, the output web tension controller can be synthesized by using the input velocity of the accumulator as control signal, whereas the second control strategy uses the web length (by moving the accumulator carriage) as control signal. In industrial applications, both control schemes are implemented. In this study, the input velocity of the accumulator is the control signal. During the regular production phase, we use the input velocity as actuator. Nevertheless, during the wound roll change, there is no control: the web moves the carriage by itself. The on/off continuous switching strategy of the controller is performed by weighting the controller output with a coefficient decreasing from 1 to 0. The control scheme is represented on Fig. 14. The PI controller C_1 has the following form:

$$C_1(s) = K_1 \frac{1 + \tau_1 s}{s} \tag{38}$$

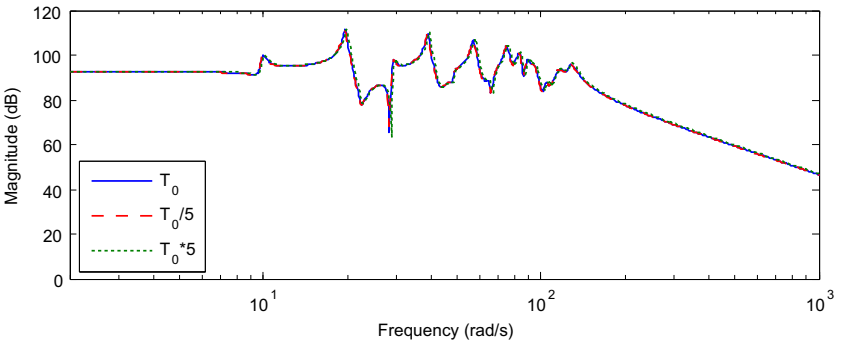

Fig. 13. Bode diagram of W_2 for different nominal web tensions.

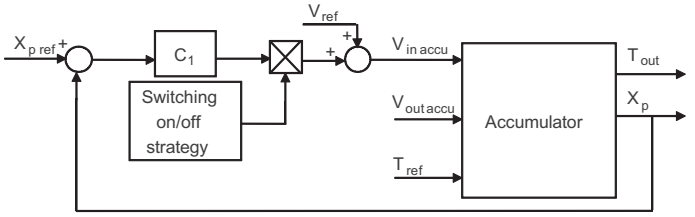

Fig. 14. Control scheme.

The PI parameters K_1 and τ_1 are determined with an optimization approach for our realistic non-linear model. Controller optimization approach can be found in Frechard et al. [27], Knittel et al. [28], Lin and Jan [29], Popov et al. [30] and Zielinski et al. [31]. The PI parameters are optimized using an evolutionary algorithm minimizing the cost function J given in (39). More details on the controllers parameters optimization can be found in Knittel et al. [20].

$$J = \int_0^{tmax} (X_p - X_{pref})^2 dt. \tag{39}$$

3.3. Simulation results

The accumulator parameters were calculated from industrial technical drawings. Moreover, the simulation results have been validated during many constructive discussions with an industrial accumulator manufacturer. The instrumentation being too expensive and very time-consuming for the accumulator manufacturer, only simulation results can be presented. However, the tendencies of our simulation results are comparable to the measurements presented in [15]. Fig. 15 presents simulation results of the modelled accumulator. The first plot shows the web velocity upstream (unwinder) and downstream the accumulator. The second plot presents the web tension at the accumulator output roll and it's reference. The plot at the bottom indicates the accumulator carriage position. One can observe on Fig. 15 that optimized PI controller ensures moderate tension variation, even during the wound roll change phase (d, e and f). The accumulator simulation sequences are:

a: The accumulator is at its nominal web length, velocity and tension.
b: The accumulator carriage is moved up to reach the maximum web length whereas the velocity is increased to maintain nominal web tension.
c: The accumulator is charged and maintained at maximum web length.
d: The input velocity decreases and the accumulator carriage is moved down to restore web and maintain the nominal web tension.
e: The input velocity is equal to zero, the accumulator carriage is moved down to restore web and maintain the nominal web tension.
f: The input velocity increases to reach the nominal velocity, the accumulator carriage is moved down to restore web and maintain the nominal web tension.
g: The accumulator is at its nominal web velocity and tension, the accumulator is maintained at a constant position to maintain a constant web length in the accumulator.

Fig. 16 presents the effects of some perturbations on the accumulator performances for another working point. The green curve shows that adding noise to the feedback signal reduces, as expected, the performances of the output tension control. Therefore, the measured signal has to be filtered during the implementation.

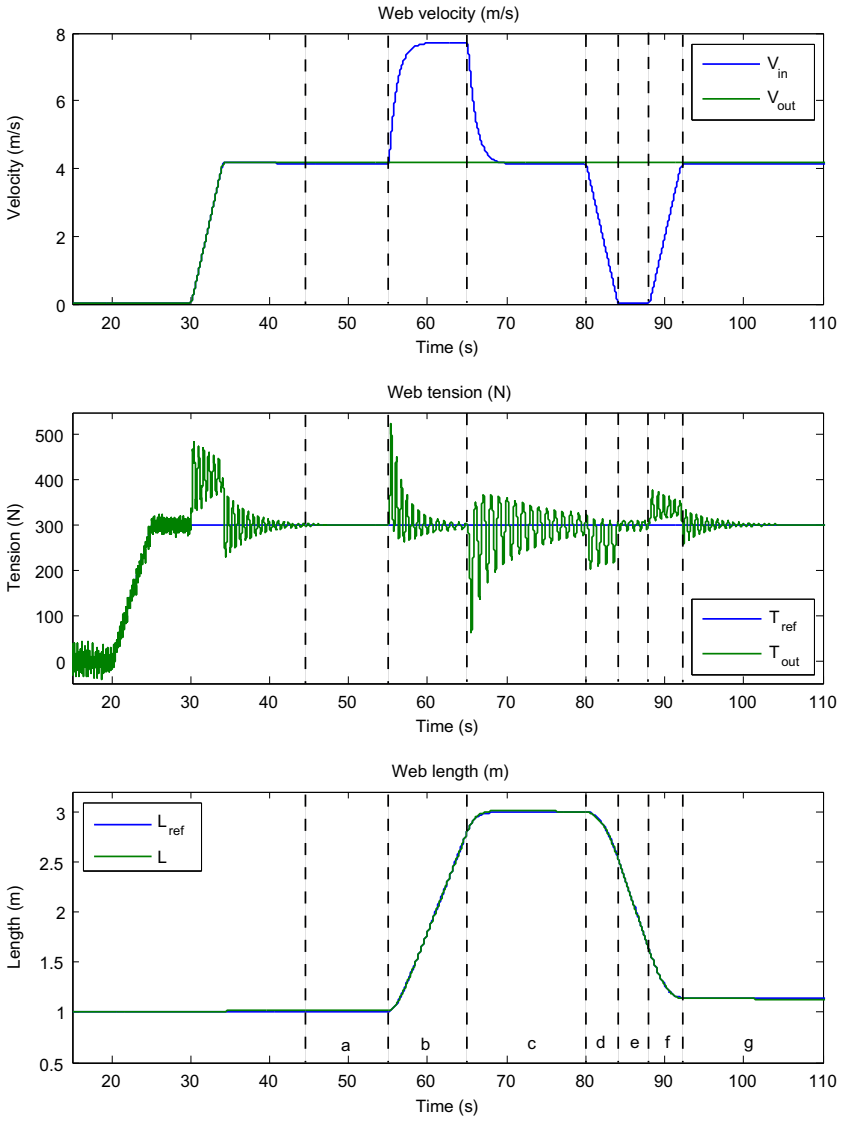

Fig. 15. Accumulator simulation results.

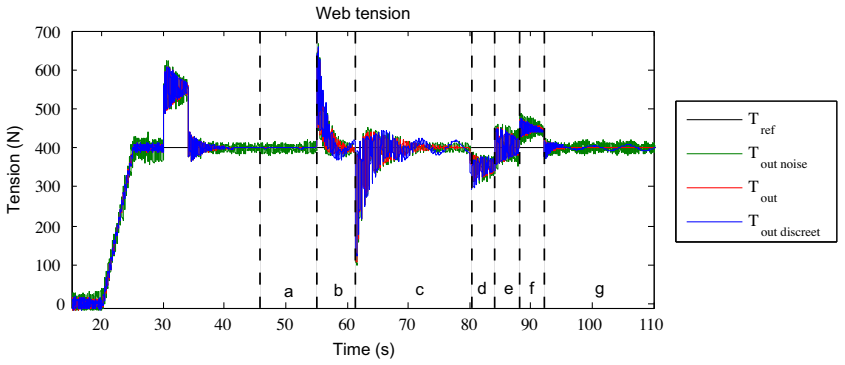

Fig. 16. Accumulator simulation results with perturbations.

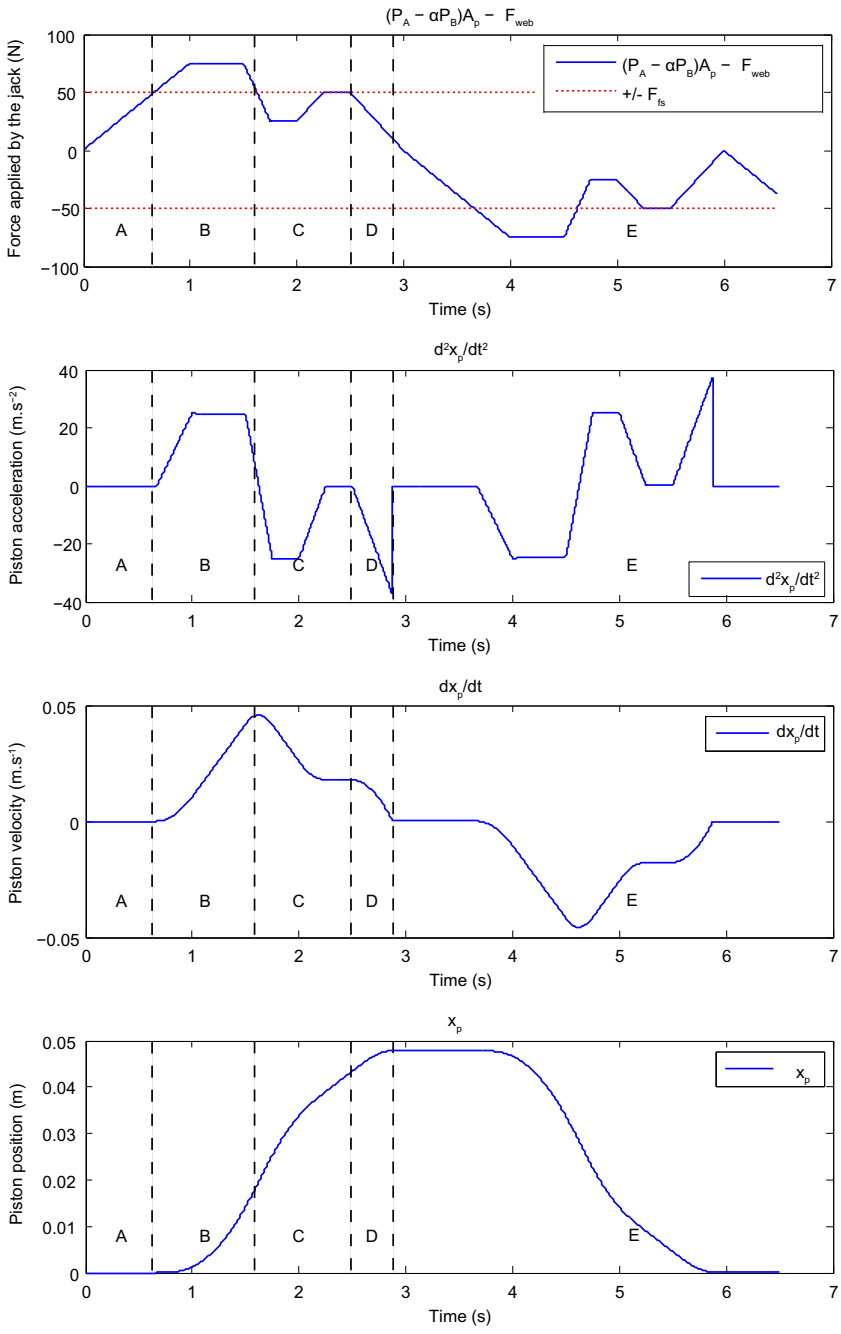

Fig. 17. Piston motion simulation including dead band due to static frictions.

In the industry, the implemented controllers are discreet (sampled): simulations are given for controllers sampled at 5 ms (which is a classical sampling time for web handling systems). We can notice a minor performances reduction. The blue[1] curve shows the results on Fig. 16. For a sampling period of 1 ms, the obtained performances are equivalent to continuous controllers.

[1] For interpretation of colour in Fig 16 , the reader is referred to the web version of this article.

4. Conclusion

This paper presents the physical equations used in the modelling of an industrial accumulator including a complete model of the pneumatic jack. The detailed nonlinear model is than programmed in Matlab/Simulink software environment which enables a model based optimization of the controllers. A linear model is deduced from the nonlinear one around a working point for frequency domain analysis. Thus, the effects of some mechanical accumulator parameters are analyzed by using simulated Bode diagrams. Time simulation results have also been presented. The nonlinear simulator reproduces the web velocity and tension in each accumulator span and therefore is devoted to accumulator design. In the next step, this model has to be used to perform a global optimization of the accumulator performances, taking into account all the influent mechanical parameters highlighted in this paper.

Acknowledgement

The authors thank Monomatic France Company for their helpful discussions. Also thanks to the Région Alsace for having partially founded this work.

Appendix A

Fig. 17.

References

[1] N. Zahlan, D. Jones, Modelling web traction on rollers, in: International Conference on Web Handling IWEB'3, Stillwater, Oklahoma, USA, 1995.
[2] G. Brandenburg, Über das dynamische Verhalten durchlaufender elastischer Stoffbahnen bei Kraftübertragung durch Coulomb'sche Reibung in einem System angetriebener, umschlungener Walzen, Ph.D. thesis, University of Munich, Germany, 1971.
[3] G. Brandenburg, Ein mathematisches Modell für eine durchlaufende elastische Stoffbahn in einem system angetriebener, umschlungener Walzen, Regelungstech. und Prozess-Datenverarbeitung 3 (1973) 69–162.
[4] A. Benlatreche, D. Knittel, E. Ostertag, Robust decentralized control strategies for large-scale web handling systems, Contr. Eng. Pract. 16 (2008) 736–750.
[5] D. Knittel, A. Arbogast, M. Vedrines, P. Pagilla, Decentralized robust control strategies with model based feedforward for elastic web winding systems, in: American Control Conference, Minneapolis, Minnesota, USA, 2006.
[6] D. Knittel, E. Laroche, D. Gigan, H. Koç, Tension control for winding systems with two-degrees-of-freedom $H\infty$ controllers, IEEE T. Industry Appl. 39 (1) (2003) 113–120.
[7] V. Gassmann, D. Knittel, P.R. Pagilla, M.-A. Bueno, $H\infty$ unwinding web tension control of a strip processing plant using a pendulum dancer, in: American Control Conference, Saint-Louis, Missouri, USA, 2009.
[8] N. Giannoccaro, A. Messina, T. Sakamoto, Updating of a lumped model for an experimental web tension control system using a multivariable optimization method, Appl. Math. Model. 34 (3) (2010) 671–683.
[9] C. Chen, K. Chang, C. Chang, Modeling and control of a web-fed machine, Appl. Math. Model. 28 (2004) 863–876.
[10] W. Wolfermann, Tension control of webs – a review of the problems and solutions in the present and future, in: International conference on Web Handling, IWEB3, Oklahoma, USA, 1995, pp. 198–229.
[11] J. Olsen, Theoretical analysis of winding mechanics, Ph.D. thesis, Norwegian University of Science and Technology 1996.
[12] V. Gassmann, Commande décentralisée robuste de systemes d'entraînement de bandes à élasticité variable, Ph.D. thesis, University of Strasbourg, Strasbourg, France, 2011.
[13] D. Knittel, L. Federlin, M. Boutaous, P. Bourgin, M. Loesch, B. Muller, Modeling and tension control of an industrial winder with dancer mechanism, in: IFAC Symposium MMM'2004, Nancy, France, 2004.
[14] H. Koç, D. Knittel, M. De Mathelin, G. Abba, C. Gauthier, Web tension control in an industrial accumulator, in: International Conference on Web Handling IWEB'99, Stillwater, Oklahoma, USA, 1999.
[15] H. Koç, D. Knittel, M. De Mathelin, C. Gauthier, G. Abba, E. Ostertag, Modeling and control of an industrial accumulator in a web transport system, in: European Control Conference ECC'99, Karlsruhe, Germany, 1999.
[16] P. Pagilla, S. Garimella, L. Dreinhoefer, E. King, Dynamics and control of accumulators in continuous strip processing lines, IEEE T. Industry Appl. 37 (3) (2001) 934–940.
[17] P. Pagilla, I. Singh, R. Dwivedula, A study on control of accumulators in web processing lines, in: American Control Conference, vol. 5, 2003, pp. 3684–3689.
[18] D. Kuhm, D. Knittel, M.-A. Bueno, Modelling and robust control of an industrial accumulator in roll to roll systems, in: 35th IEEE Annual Conference on Industrial Electronics, Porto, Portugal, 2009, pp. 1645–1650.
[19] D. Kuhm, D. Knittel, New design of robust industrial accumulator for elastic webs, in: 18th World Congress of the International Federation of Automatic Control (IFAC), Milan, Italy, 2011.
[20] D. Knittel, D. Kuhm, Multidisciplinary design optimization of an accumulator for a large elasticity range of flexible webs, in: Third International Conference on Multidisciplinary Design Optimization and Applications, Paris, France, 2010.
[21] H. Koç, Modélisation et commande robuste d'un systéme d'entrainement de bande flexible, Ph.D. thesis, University of Strasbourg, France, 2000.
[22] H. KoKoç, D. Knittel, M. De Mathelin, G. Abba, Modeling and robust control of winding systems for elastic webs, IEEE T. Control Syst. Tech. 10 (2) (2002) 197–206.
[23] G. Kim, H. Kim, J. Shin, J. Kim, Nonlinear modeling and control of servo pneumatic actuators, ISIJ Int. 48 (6) (2008) 799–808.
[24] K. Hamiti, A. Voda-Besançon, H. Roux-Buisson, Position control of a pneumatic actuator under the influence of stiction, Contr. Eng. Pract. 4 (8) (1996) 1079–1088.
[25] R. Zhihong, G. Bone, Nonlinear modeling and control of servo pneumatic actuators, IEEE T. Contr. Syst. Tech. 16 (3) (2008) 562–569.
[26] M. Jelali, A. Kroll, Hydraulic servo-systems: modelling, Ident. Control (2002).
[27] J. Frechard, D. Knittel, P. Dessagne, J. Pellé, G. Gaudiot, J. Caspar, G. Heitz, Modelling and fast position control of a new unwinding-winding mechanism design, in: Electrimacs 2011, Cergy-Pontoise, France, 2011.
[28] D. Knittel, J. Frechard, M. Vedrines, Multi-objective optimization for manufacturing process design: application in roll-to-roll systems, in: Third International Conference on Multidisciplinary Design Optimization and Applications, Paris, France, 2010.

[29] C.L. Lin, H.Y. Jan, Multi objective pid control for a linear brushless dc motor: an evolutionary approach, in: IEE Proceedings of Electrical Power and Applications, vol. 149, 2002.
[30] A. Popov, A. Farag, H. Werner, Tuning of a pid controller using a multi-objective optimization technique applied to a neutralization plant, in: European Control Conference, Sevile, Spain, 2005.
[31] K. Zielinski, M. Joost, R. Laur, B. Orlik, Comparison of differential evolution and particle swarm optimisation for the optimisation of a pi cascade control, in: IEEE Congress on Evolutionary Computation, Hong Kong, China, 2008.